Acta Metallurgica, Vol. 26, pp. 815–825. Pergamon Press, 1978. Printed in Great Britain

ORDERING IN AN OFF-STOICHIOMETRIC Ni–Mo ALLOY

L. A. NESBIT and D. E. LAUGHLIN

Carnegie-Mellon University, Department of Metallurgy and Materials Science, Pittsburgh, PA 15213, U.S.A.

(*Received* 6 *January* 1977)

Abstract—The various mechanisms of the ordering transformation in an off-stoichiometric Ni–Mo alloy have been studied by transmission electron microscopy. We have observed that the supersaturated solid solution of Mo in Ni decomposes into the terminal solid solution and the ordered β (Dla) phase by two distinct mechanisms. At 750°C, the alloy decomposes by homogeneous nucleation, while at larger undercoolings (at 700°C) the process occurs continuously, by a mechanism that has been termed spinodal ordering. Direct space, as well as reciprocal space, results are presented, and interpreted in terms of the various models for ordering transformations. The diffuse intensity maxima that occur at the $\{1\frac{1}{2}0\}$ positions in reciprocal space have also been studied, and the results are discussed in terms of short range order models.

Résumé—On a étudié par microscopie électronique en transmission les divers mécanismes de la mise en ordre d'un alliage Ni–Mo non stoechiométrique. On a observé que la solution solide sursaturée de Mo dans le Ni se décomposait en la solution solide terminale et la phase ordonnée β (Dla) selon deux mécanismes distincts. A 750°C, l'alliage se décompose par germination homogène, alors que, pour de plus fortes surfusions (à 700°C), le processus est continu; l'on a appelé ce second mécanisme mise en ordre spinodale. On présente des résultats, dans l'espace direct et dans l'espace réciproque, que l'on interprete à l'aide des divers modèles de mise en ordre. On étudie également les maximums d'intensité diffuse que se produisent aux positions $\{1\frac{1}{2}0\}$ de l'espace réciproque, et l'on discute cette observation à l'aide des modèles de l'ordre à courte distance.

Zusammenfassung—Mittels Durchstrahlungselektronenmikroskopie wurden die verschiedenen Mechanismen der Ordnungsumwandlung in einer nicht-stöchiometrischen Legierung Ni–Mo untersucht. Wir haben beobachtet, daß die übersättigte Lösung von Mo in Ni mit zwei Mechanismen in die endgültige feste Lösung und die geordnete β-Phase (D1a) zerfällt. Bei 750°C zerfällt die Legierung durch homogene Keimbildung, wohingegen bei stärkerer Unterkühlung (bei 700°C) der Prozess kontinuierlich über einen Mechanismus abläuft, der spinodale Ordnungseinstellung genannt wurde. Ergebnisse aus dem Orts- und dem reziproken Raum werden vorgelegt und auf der Grundlage der verschiedenen Modelle für die Ordnungsumwandlung diskutiert. Außerdem wurden die diffusen Intensitätsmaxima bei den $\{1\frac{1}{2}0\}$-Positionen ebenfalls untersucht; die Ergebnisse werden anhand von Nahordnungsmodellen diskutiert.

I. INTRODUCTION

Over the past several years most research on ordering transformations in binary alloys has centered on alloys of stoichiometric composition for which the transformation reaction may be written as

$$\alpha' \rightarrow \beta, \qquad (1)$$

where α' denotes the high temperature disordered solid solution phase and β designates the low temperature ordered phase. Such stoichiometric alloys accommodate few exploitable applications due to their inherent brittleness. Of greater practical significance are alloys of off-stoichiometric composition, for which the ordering reaction is summarized by the equation

$$\alpha' \rightarrow \alpha + \beta, \qquad (2)$$

where α' is the supersaturated solid solution, α is the disordered terminal solid solution matrix phase in equilibrium with the ordered β precipitate phase. Such reactions occur in superalloys and other age-hardening systems. A better understanding of the various mechanisms of the ordering reaction, as well as the resulting microstructures, will aid in the control of the corresponding mechanical properties. This paper describes certain microstructural findings in the Ni–Mo system. Work on correlating the microstructural features to the mechanical properties is in progress and will be the subject of a subsequent paper.

An additional impetus for investigating reactions of the form of equation (2) is that the ordering process occurs at a slower rate than in a corresponding reaction described by equation (1). This is because fewer solute atoms are present, hence diffusion must occur over a larger distance in order for the ordered phase to form. Thus, the use of an off-stoichiometric alloy is especially beneficial in studying the early stages of the transformation and in determining the exact sequence of events which occur both in direct space and in reciprocal space.

In the past, the study of the ordering transformation in the Ni–Mo system has been hindered by the rapidity of the ordering reaction, so that heat treatments of a few seconds [1] are often too long to determine the early stages of the reaction. Also insufficiently rapid quenching rates may lead to misconceptions concerning the state of the alloy above the critical temperature. An investigation of an off-stoichiometric alloy is thus expected to enhance the understanding of the various ordering mechanisms in the corresponding stoichiometric alloy.

Gibbs [2] was the first to distinguish between two modes of tranformation which may occur in physical systems; namely, (i) those which are large in degree and small in extent, and (ii) those which are small in degree and large in extent. Christian [3] makes a similar distinction in metallic systems, labeling the former mode a *heterogeneous transformation* and the latter mode a *homogeneous transformation.*

For a transformation reaction of the form of equation (2), the ordered β phase may form heterogeneously from disordered supersaturated α' solid solution by homogeneous and/or heterogeneous nucleation. Alternatively the ordered phase may form homogeneously throughout the α' phase by one of the following mechanisms: (1) spinodal decomposition (clustering) followed by ordering within the solute region [4–8]; (2) spinodal ordering, [8] in which "the early stage spinodal structure is not the final equilibrium one" [9]; (3) continuous ordering, [8] in which the "final equilibrium structure evolves continuously from a low amplitude quasi-homogeneous concentration wave" [9].

In order to distinguish between the homogeneous and heterogeneous modes of transformation, it is necessary to observe the initial stages of the formation of the second phase. Attempts to determine the mode of the transformation based on microstructures and diffraction patterns from specimens aged at longer times may result in an erroneous classification, as similar microstructures and diffraction patterns may develop from both modes [10].

The initial microstructure of a heterogeneous transformation may be characterized by microscopically distinct regions of fully transformed precipitates in the untransformed parent matrix. The transformed regions are usually relatively small compared to the crystal in which they nucleate, and a distinct interface separates each nucleus from the parent matrix. In a diffraction pattern the reciprocal lattice of the precipitate phase will appear suddenly or discontinuously with isothermal aging time; that is, the reciprocal lattice of the precipitate will not gradually develop from the reciprocal lattice of the matrix phase. Thus for a heterogeneous order–disorder transformation, the superlattice reflections should appear discontinuously after a certain aging time.

A homogeneous transformation occurs simultaneously throughout the entire parent matrix by means of a spinodal mechanism in which a composition wave or fluctuation becomes unstable below a critical temperature. Implicit in such a transformation is zero or near zero surface energy between the parent and precipitate phases so that no distinct interface initially exists between the two phases. Also, if there is sufficient lattice misfit between the parent and product phases, the development of a tweed microstructure would be consistent with, but not necessarily indicative of, a homogeneous transformation. In reciprocal space, one would expect a gradual development of the second phase reciprocal lattice. For an order–disorder transformation the long-range order (LRO) might develop continuously from any existing short-range order (SRO), so that a continuous transfer of diffracted intensity from the SRO intensity maxima to the LRO position would be observed during the aging process.

The purpose of this investigation is to document the various microstructural and reciprocal lattice features of an off-stoichiometric Ni–Mo alloy in which an ordered β phase precipitates from a disordered supersaturated α' phase at two different isothermal aging temperatures. From these results the mode of transformation at each temperature will be ascertained.

The off-stoichiometric Ni–Mo alloy chosen for this investigation was Ni–16.7 at.% Mo (24.7 wt.% Mo). The composition of the alloy as well as the temperatures at which it was isothermally aged are shown in Fig. 1. Below 835°C (1108 K) the alloy consists of two phases, the terminal solid solution α (f.c.c.) and the ordered β phase (Ni_4Mo) which has a Dla crystal structure [11]. The crystallography of Ni_4Mo has been extensively reviewed by previous authors [1, 12] and will not be presented in detail in this paper. One aspect of the crystallography, which is pertinent, is

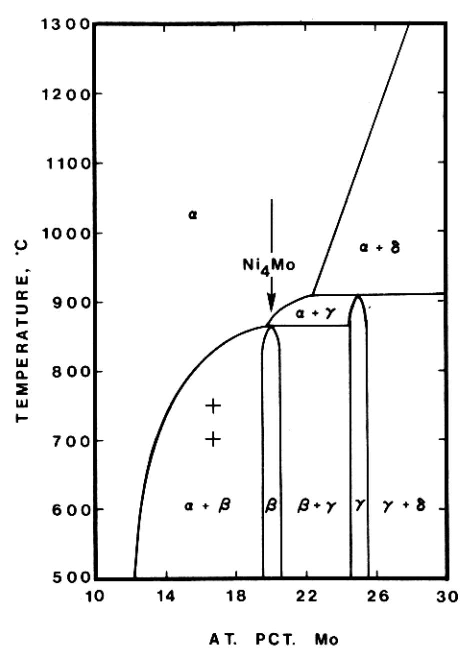

Fig. 1. Partial Ni–Mo phase diagram showing the composition of the alloy at Ni–16.7 at.% Mo (24.7 wt.% Mo) relative to the stoichiometric β phase at Ni–20 at.% Mo (Ni_4Mo). Also shown are the relative positions of the aging temperatures, 700 and 750°C, in the two-phase field.

the crystallographic relationship of a coherent β precipitate relative to the matrix α phase. The Bravais lattice of the Dla structure is body-centered tetragonal (b.c.t.) with $c/a = 0.623$. When coherent with the matrix, the c-axis of the Dla structure lies along one of the cube directions of the f.c.c. lattice, while the two a axes lie along two perpendicular $\langle 130 \rangle_{\text{f.c.c.}}$ directions. Since four $\langle 130 \rangle_{\text{f.c.c.}}$ directions lie in the plane perpendicular to a $\langle 001 \rangle_{\text{f.c.c.}}$, two possible orientation variants exist for each c axis so that six orientation variants of the Dla structure may occur in the microstructure.

Previous work on Ni–Mo alloys of similar composition by Spruiell, Ruch and Brooks [13] dealt with the dependence of certain mechanical properties on particle size of presumably homogeneously nucleated β precipitates, but they did not investigate the various possible transformation mechanisms.

II. EXPERIMENTAL PROCEDURE

The Ni–16.7 at.% Mo alloy was prepared from Ni and Mo powders, each with an initial purity of 99.9%. The powders were mechanically mixed, compressed into a cylinder button, and then arc-melted three times in an argon atmosphere. The buttons were turned over between each melting to increase their homogeneity. The resulting alloy was homogenized at 1152°C (1425 K) in a quartz capsule and then subjected to a series of cold rolling and recrystallization annealing treatments until optical microscopy showed large equiaxed grains (0.2–0.3 mm in diameter) in the final alloy of thickness 0.25–0.38 mm (10–15 mills).

One centimeter square specimens received a final homogenization anneal at 1000°C (1273 K) for 2 h and then were down-quenched [14] to the isothermal aging temperature. The specimens were aged in the molten lead at either 700 or 750°C (973 or 1023 K) for times ranging from 30 s to 30 min and then quenched in ice-water. Specimens requiring aging times up to 10^4 min were stripped of any adhering lead and wrapped in titanium foil for further heat treatment at the same temperature in a flowing argon gas furnace.

Thin foils for transmission electron microscopy were prepared by the twin-jet method using a solution of one part HNO_3 in two parts methanol at -20 to -30°C (253-243 K). The transmission electron microscopy was performed on a JEM-100B with a double tilt stage, capable of $\pm 36°$ on one axis and $\pm 60°$ on a perpendicular axis.

III. RESULTS

(a) The as-quenched state

Specimens directly quenched from the homogenization temperature into ice-water display diffuse SRO intensity maxima at the $\frac{1}{4}\{420\}$ positions in reciprocal space. Within a square sector formed by four fundamental reflections on a [001] pattern, the SRO intensity maxima lie in a faint ring of diffracted intensity as shown in Fig. 2(a). Figure 2(b) shows that the SRO spots on a [112] pattern appear symmetrical in the as-quenched condition.

No transformation microstructure is observed in the corresponding bright-field microstructure and attempts to image in dark-field precipitates or microdomains from the $\frac{1}{4}\{420\}$ intensity maxima proved unsuccessful.

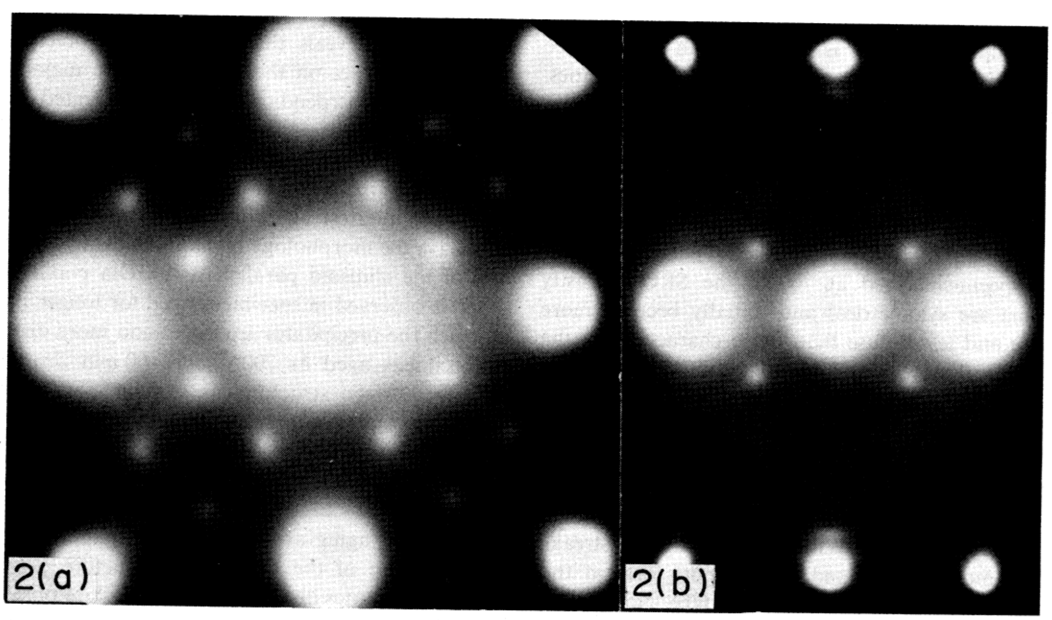

Fig. 2. Diffraction patterns of Ni–16.7 at.% Mo along the (a) [001] and (b) [112] zone axes in the as-quenched condition. Each group of four SRO intensity maxima lie in a ring of diffuse intensity in (a).

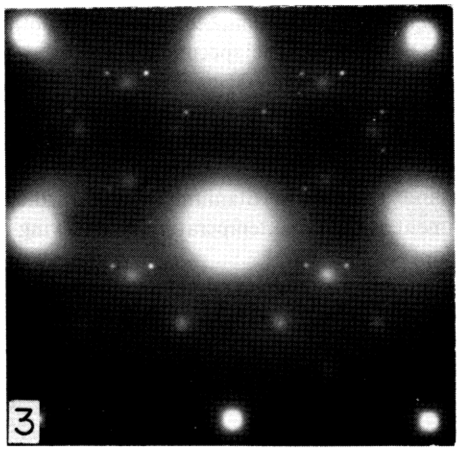

Fig. 3. The [001] diffraction pattern of Ni–16.7 at.% Mo aged at 750°C for 20 min. Sharp LRO reflections are observed at the $\frac{1}{5}\{420\}$ positions.

(*b*) *The transformation at* 750°C

Specimens of the alloy aged at 750°C for short times, display SRO intensity maxima which are more intense and less diffuse than those typifying the as-quenched condition. The SRO spots on both the [001] and the [112] diffraction patterns have a symmetrical intensity profile throughout the aging process.

Sharp LRO spots appear suddenly or discontinuously at the $\frac{1}{5}\{420\}$ positions after an aging time of 20 min, as shown in Fig. 3. The existence of the LRO spots corresponds to the presence of ordered Ni_4Mo precipitates as shown in the bright-field and dark-field microstructures in Figs. 4(a) and (b), respectively. These initial precipitates appear as rounded squares, when observed along the Dla *c*-axis, and are approximately 5–10 nm in size. The distribution of the precipitates is random, with no evidence that precipitation occurs on structural heterogeneities.

With continued aging, the Ni_4Mo precipitates become faceted on the {100} planes and aligned in the ⟨100⟩ directions of the matrix. Also, the SRO intensity maxima eventually completely disappear.

(*c*) *The transformation at* 700°C

In specimens aged at 700°C, the SRO intensity maxima are symmetrical and initially become more intense and less diffuse than those characterizing the as-quenched state. See Fig. 5 and compare with Fig. 2. For aging times as short as 0.5 min, faint streaks of diffracted intensity commence to form only on the {112} reciprocal lattice planes. These streaks lie in the ⟨420⟩ directions between two $\frac{1}{5}\{420\}$ (LRO) positions of the same orientation variant and pass through a $\frac{1}{4}\{420\}$ (SRO) position. With further aging, the streaks become more intense, and diffuse spots form at the $\frac{1}{5}\{420\}$ positions. See Figs. 5(b) and 6(b). Notice also in Fig. 5(b) that the SRO spot is more intense than the faint LRO spot. Although the diffuse streaks pass through the $\frac{1}{4}\{420\}$ positions, the SRO intensity maxima remain symmetrical throughout the aging process. In direct space, there is no evidence of a transformation microstructure corresponding to these streaks on the (112) reciprocal lattice plane.

No diffuse streaks are observed on the (001) reciprocal lattice plane until after an aging time of 10 min, when diffuse intensity is observed between the $\frac{1}{4}\{420\}$ and the $\frac{1}{5}\{420\}$ positions as shown in Fig. 6(a). Despite the presence of this diffuse intensity, the intensity profile of the SRO spots is symmetrical and remains symmetrical throughout the entire aging process.

Concurrent with the existence of the diffuse intensity between the SRO and the LRO positions on the [001] diffraction pattern is the presence of a faint {110} tweed microstructure [8]. This tweed microstructure is observed throughout the specimen and becomes more pronounced with further aging (see Fig. 7). The periodicity of the tweed modulations along the traces of the {110} planes is 10–15 nm. No distinct Ni_4Mo precipitates are observed in the bright-field microstructures of Fig. 7, but imaging the superlattice reflections on the [001] diffraction pattern reveals faint Ni_4Mo precipitates about 2–5 nm in size throughout the dark-field microstructure after aging for 30 min (see Fig. 8).

Figures 9(a) and (b) display the [001] and [112] diffraction patterns corresponding to the tweed microstructures in Fig. 7, and to the dark-field microstructure in Fig. 8. Distinct LRO and SRO intensity maxima are observed in both diffraction patterns, with most of the diffuse intensity between the LRO and the SRO positions having disappeared. Although the superlattice reflections on the [001] diffraction pattern are symmetrical, those on the [112] pattern are elongated in a ⟨420⟩ direction. Imaging the superlattice reflections on the [112] pattern individually in dark field reveals that the resulting precipitates project as ellipses on the (112), with the major axis of the ellipses perpendicular to the elongated direction of the corresponding superlattice reflection. Thus the elliptical shape of the superlattice reflections on the [112] diffraction pattern arises from the shape of the precipitates. The precipitates themselves probably have the morphology of ellipsoids with the major axis of the ellipsoid parallel to the Dla *c*-axis. This shape is observed in specimens aged for longer times, in which the precipitates are larger and more distinct.

Specimens aged at 700°C for 100 min display a coarsened tweed structure, as seen in Fig. 10. The ordered precipitates corresponding to this microstructure are about 10 nm in size. In the reciprocal lattice, the SRO intensity maxima have completely disappeared.

Continued aging at 700°C results in the complete disappearance of the tweed microstructure, so that after 1000 minutes distinct β precipitates are observed in both the bright field and dark field micrographs of Fig. 11. The precipitates have a square cross-section as observed along their *c*-axes or identically

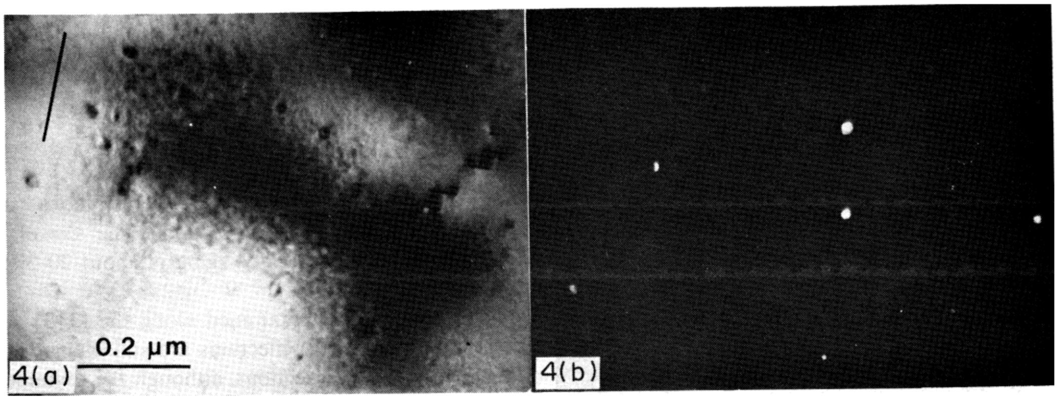

Fig. 4. Ni–16.7 at.% Mo aged at 750°C for 20 min. Distinct randomly spaced β precipitates are observed along the [001] zone axis in (a) bright field and (b) dark field. The [100] direction is also shown in (a).

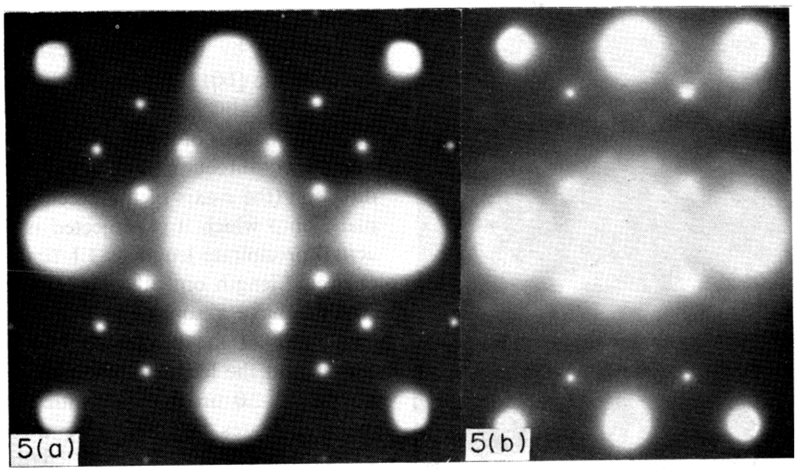

Fig. 5. The (a) [001] and (b) [112] diffraction patterns of Ni–16.7 at.% Mo aged at 700°C for 5 min. The SRO intensity maxima are less diffuse and more intense than those in Fig. 2. Faint streaks are observed in the ⟨420⟩ directions on the [112] pattern in (b).

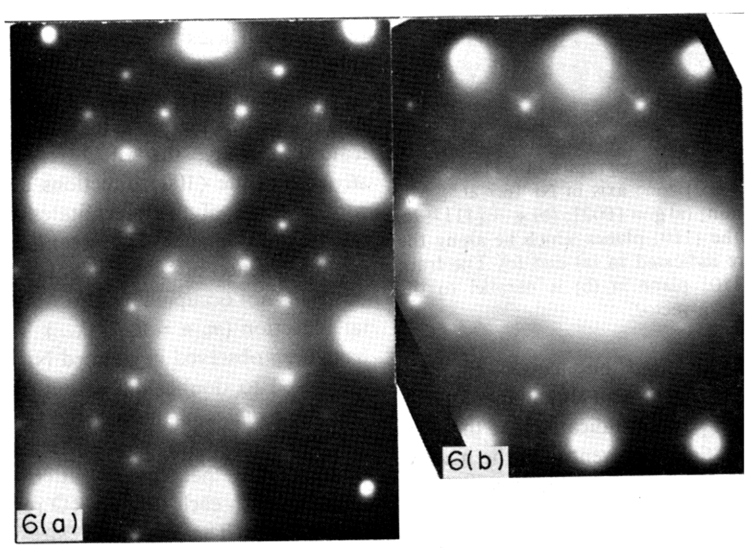

Fig. 6. The (a) [001] and (b) [112] diffraction patterns of Ni–16.7 at.% Mo aged at 700°C for 10 min. Diffuse intensity is observed between the symmetrical SRO intensity contours and the LRO positions on the [001] pattern in (a).

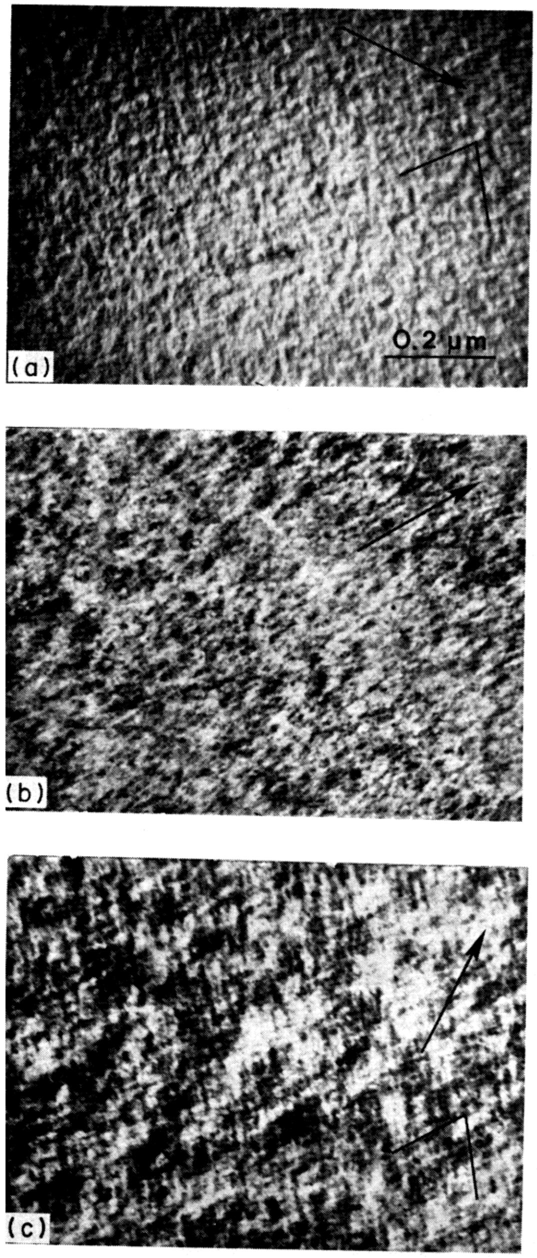

Fig. 7. Bright field electron micrographs of ⟨110⟩ tweed as observed near the [110] zone axis in Ni–16.7 at.% Mo aged at 700°C for 30 min; (a) $\mathbf{g} = [002]$; (b) $\mathbf{g} = [1\bar{1}\bar{1}]$; (c) $\mathbf{g} = [2\bar{2}0]$. Traces of the {110} planes which lie along the tweed modulations are indicated in (a) and (c). The trace of the appropriate {110} plane in (b) is parallel to the **g**-vector.

along the [001] zone axis, and the facets of the precipitates lie along the (100) and (010) planes of the matrix. The diffraction pattern indicates that the precipitates are at least initially coherent with the matrix, so that the following crystallographic relationship must be true for the two orientation variants of the β phase as observed on the (001) diffraction pattern: for

$$[001]_\beta \| [001]_\alpha,$$

then

$$(100)_\beta \| (310)_\alpha \text{ and } (010)_\beta \| (\bar{1}30)_\alpha$$

or

$$(100)_\beta \| (3\bar{1}0)_\alpha \text{ and } (010)_\beta \| (130)_\alpha.$$

In addition, an alignment of the precipitates exists in the $[100]_\alpha$ and $[010]_\alpha$ directions. The size of the precipitates at this stage of aging is about 20–30 nm on a side.

If the specimen is examined along the [112] zone axis, the superlattice reflections are still elongated in one of two ⟨420⟩ directions, although the asymmetry of the reflections is not as pronounced as after only 30 min aging time. Imaging the LRO spots individually in dark field reveals the general shape of the precipitates which is represented by the schematic drawing in Fig. 12. The precipitates possess four-fold symmetry about their crystallographic *c*-axes, which is indicated by the symmetrical superlattice reflections on the [001] diffraction pattern. Trace analysis of the [112] diffraction pattern shows that the trace of the major axis of the precipitate lies along the trace of a ⟨100⟩ direction. The angle between this ⟨100⟩ direction (the *c*-axis of the precipitate) and the {112} plane onto which it is projected is 65.9°, so that the actual precipitate length is 1.1 times greater than its projected length onto the {112} plane. Thus the precipitates have a square cross-section normal to the major axis of the precipitate (the *c*-axis of the Dla lattice) and the length of the precipitates is approximately 1.5–2.0 times their width. The dimensions of the precipitates for this aging treatment are about 20 nm in width and 40 nm in length.

The microstructure, after 10,000 min aging at 700°C, is shown in Fig. 13. The faceted interface of the precipitates are still parallel to the $\{100\}_\alpha$ planes and the microstructure reveals a definite alignment of the β particles in the ⟨100⟩ directions. The size of these particles is approximately 30–50 nm on a side.

The diffraction pattern corresponding to Figs. 13(a) and (b), shown in Fig. 13(c), displays two interesting features. Firstly, the LRO reflections are slightly streaked in the ⟨100⟩ directions due to the generally square shape of the precipitates, which are faceted on the {100} planes. The second noteworthy feature is the presence of "extra" spots at all $\{m/5, n/5, 0\}$ positions not occupied by a superlattice or fundamental reflection (m, $n = 0, 1, 2, \ldots$). These "extra" spots have been observed in ordered Ni_4Mo and have been attributed to double diffraction from different overlapping *domains* of the ordered structure [12].

Indeed, the "extra" spot pattern can be constructed by translating the primary pattern so that the origin coincides with each of the LRO reflections of the primary pattern. Therefore the "extra" spots in this alloy are due to the diffracted superlattice reflection from one *precipitate* being diffracted again by a second *precipitate*.

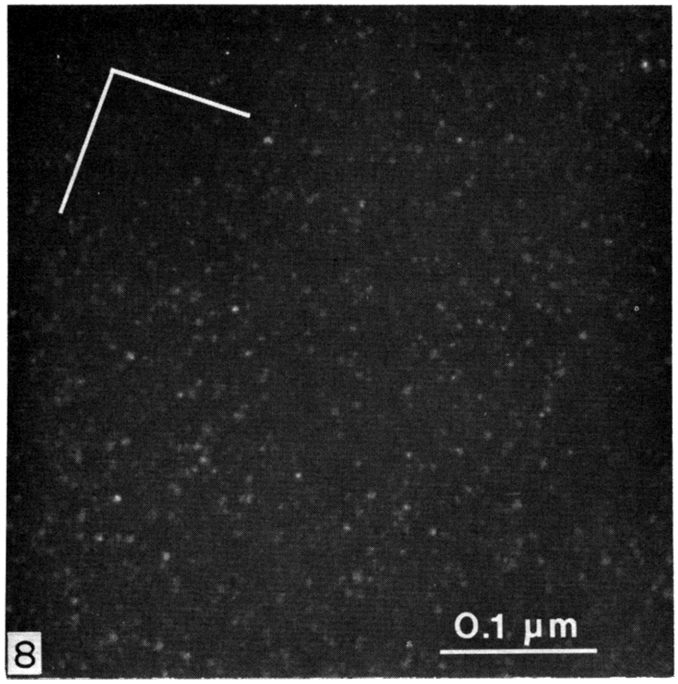

Fig. 8. The β (Ni_4Mo) precipitates as observed in dark field by imaging the two LRO variants in the [001] diffraction pattern of Ni–16.7 at.% Mo aged at 700°C for 30 min. Also shown are the [100] and [010] directions

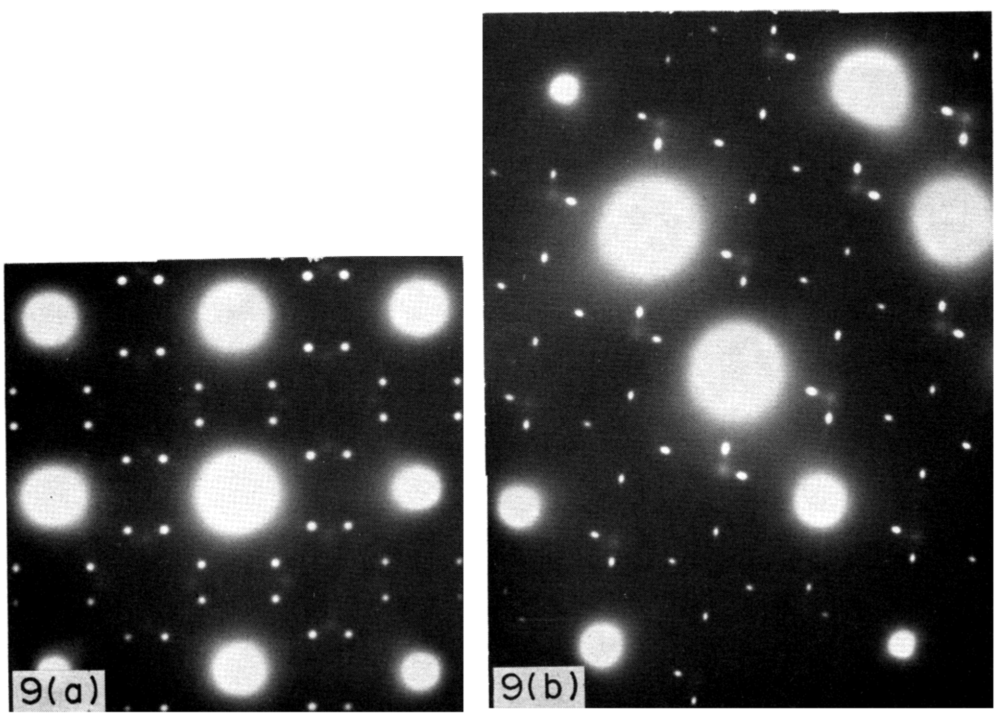

Fig. 9. Ni–16.7 at.% Mo aged at 700°C for 30 min. (a) [001] diffraction pattern and (b) [112] diffraction pattern. Symmetrical SRO intensity contours are observed in both diffraction patterns. The LRO reflections are symmetrical in the [001] pattern, asymmetrical in the [112] pattern.

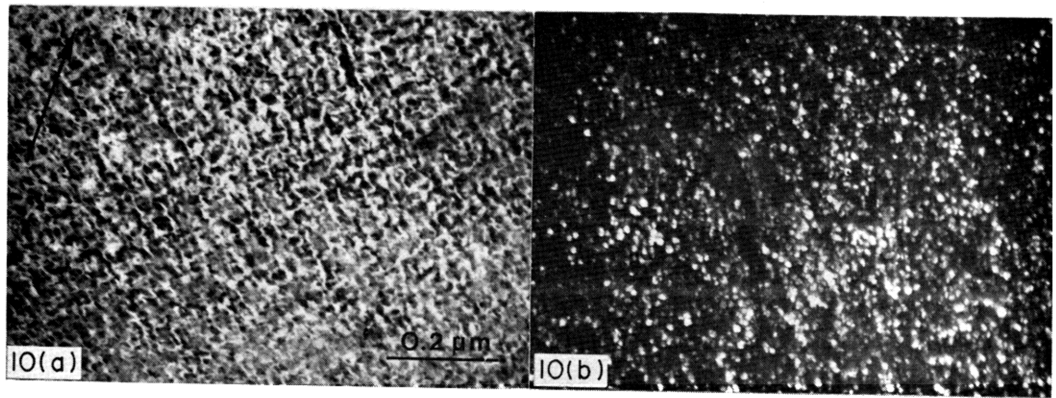

Fig. 10. Ni–16.7 at.% Mo aged at 700°C for 100 min as observed along the [001] zone axis in (a) bright field and (b) dark field by imaging two of the LRO variants. The **g**-vector, **g** = [200], is shown in (a).

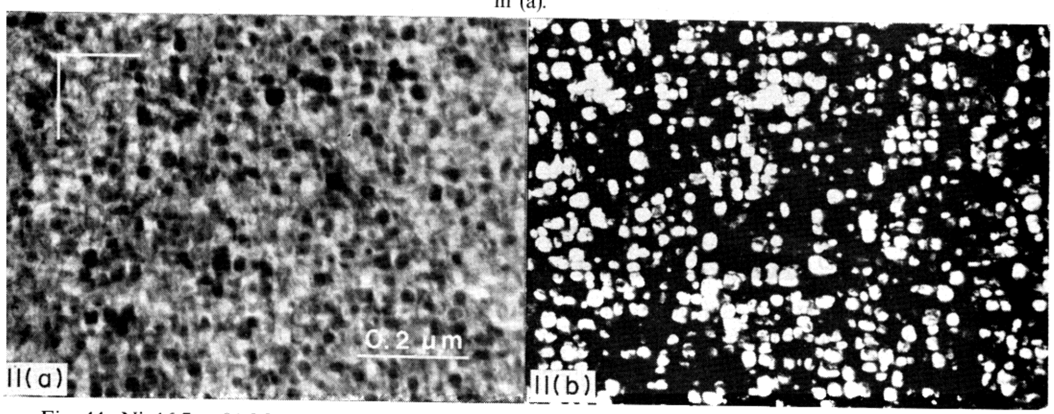

Fig. 11. Ni–16.7 at.% Mo aged at 700°C for 1000 min as observed along the [001] zones axis in (a) bright field and (b) dark field by imaging two of the LRO variants. The [100] and [010] directions are indicated in (a).

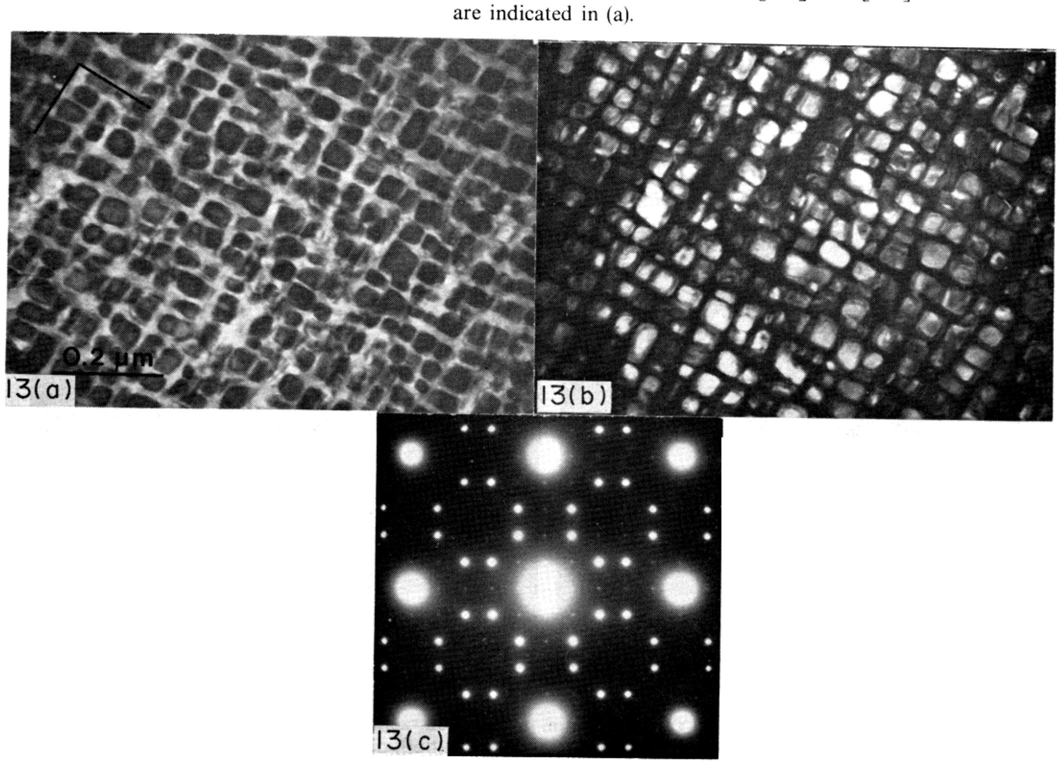

Fig. 13. Ni–16.7 at.% Mo aged at 700°C for 10,000 min as observed along the [001] zone axis in (a) bright field and (b) dark field by imaging two of the LRO variants. The [100] and [010] directions indicated in (a). The corresponding [001] diffraction pattern is shown in (c).

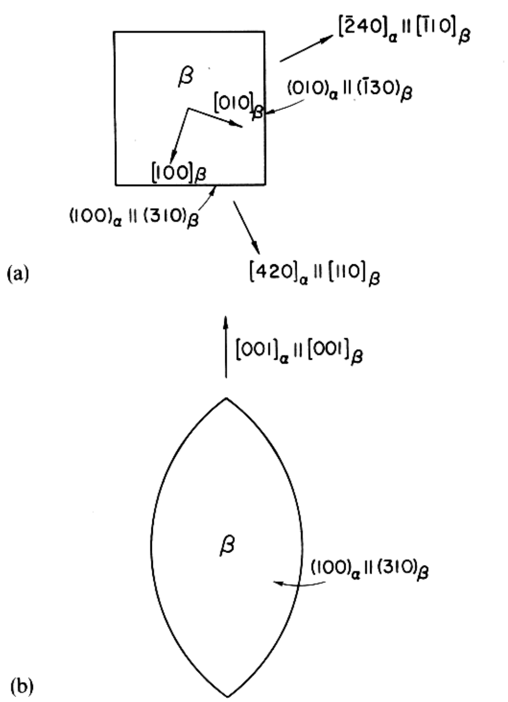

Fig. 12. Ni_4Mo (β) precipitate morphology after aging at 700°C for 1000 min; (a) view along $[001]_\alpha \| [001]_\beta$, and (b) face view of the precipitate.

IV. DISCUSSION

(a) *The as-quenched state*

The physical interpretation of the SRO intensity maxima in Ni_4Mo has been the subject of much discussion in the recent literature. The two basic viewpoints concerning the SRO intensity maxima are the microdomain theory, as described by Thomas and coworkers [1, 15–17] and by Ruedl, Delavignette and Amelinckx [12] and the statistical thermodynamic model, as outlined by Clapp and Moss [18, 19] and supported by Chakravarti *et al.* [20] Our qualitative transmission electron microscopy results will be discussed in terms of these two models.

In the as-quenched state of our alloy, the SRO intensity maxima do not possess circular symmetry as observed on the (001) reciprocal lattice plane in Fig. 2(a). This diffraction pattern is similar to that of as-quenched Ni_4Mo obtained by DeRidder, Van Tendeloo and Amelinckx [21]. With relatively short aging times at both 700 and 750°C, the SRO spots in our alloy become symmetrical on both the {112} and {100} reciprocal lattice planes, and thus spherical in reciprocal space. Although streaks develop from the SRO spots upon aging at 700°C, sufficient defocusing of the second condensor lens demonstrates that the SRO spots are more intense than the streaks, and the intensity at the $\frac{1}{4}\{420\}$ reflections remains symmetrical throughout the aging process (see Fig. 6a and b).

The sphericity of the SRO intensity maxima indicates that they result from a minimum in $V(k)$ at the special points $\{1\frac{1}{2}0\}$ in reciprocal space. $V(k)$ is the Fourier transform of the pair-wise interatomic potential as a function of k, the reciprocal lattice position vector. This explanation of the shape of the SRO reflections is consistent with the statistical thermodynamic model as explained by Clapp and Moss [18, 19] and by de Fontaine [9]. The change in the intensity and diffuseness of the SRO spots from the as-quenched to that of later aging times results from the minimum in $V(k)$ producing a maximum in the amplification rate of the $\langle 1\frac{1}{2}0 \rangle$ concentration waves.

In an earlier study of as-quenched stoichiometric Ni_4Mo, [1] the investigators reported evidence for the presence of microdomains which give rise to the SRO reflections and to weak intensity maxima near, but not exactly at, the equilibrium positions of the superlattice reflections of the fully ordered Ni_4Mo. No such weak intensity maxima are observed in the as-quenched state of our alloy. However aging at 700°C for short times produce streaks in the $\langle 420 \rangle$ directions which pass through the same positions as these weak inensity maxima. Thus any streaks in the $\langle 420 \rangle$ directions or weak intensity near the LRO positions should not be interpreted as being indicative of the SRO structure. Rather such intensity should be viewed as being due to the gradual development of the LRO structure from the $\frac{1}{4}\langle 420 \rangle$ concentration waves.

Thus the sphericity of the SRO reflections throughout the aging process, the lack of any streaks in the $\langle 420 \rangle$ directions in the as-quenched state, and the absence of particles in dark field from the SRO spots together support the statistical thermodynamic model as proposed by Clapp and Moss for the physical interpretation of the SRO structure. Subsequently de Fontaine [9] has suggested a type of "average cluster" consistent with the Clapp and Moss model which takes into account the $\langle 1\frac{1}{2}0 \rangle$ concentration waves.

(b) *The ordering transformation*

The description of the ordering processes in the previous section demonstrates that essential differences exist in the initial mechanisms of the ordering transformation at 700 and 750°C. At 750°C, the $\frac{1}{4}\{420\}$ SRO reflections are more intense and less diffuse than those in the as-quenched state, but they do not seem to be connected with the sudden appearance of the $\frac{1}{5}\{420\}$ LRO reflections after 20 min aging time. The corresponding distinct precipitates imaged in both bright and dark fields are randomly distributed throughout the matrix, indicating that the ordering reaction has occurred as a discontinuous or *heterogeneous transformation* by means of homogeneous or uniform nucleation (realizing of course that very small defects *may* have influenced the nucleation event).

The transformation at 700°C has numerous characteristics, distinguishing it from the transformation at 750°C. Although the $\frac{1}{4}\{420\}$ SRO reflections are also more intense and less diffuse than those of the as-quenched condition, the $\frac{1}{5}\{420\}$ LRO reflections form by a continuous transfer of diffracted intensity from the $\frac{1}{4}\{420\}$ SRO intensity maxima. This suggests that unlike the transformation at 750°C, at 700°C the SRO structure plays an integral role in the formation of the long-range ordered Dla structure. This continuous transfer or streaking of intensity is first observed on $\langle 112 \rangle$ diffraction patterns for aging times as short as 0.5 min. The streaks lie along two $\langle 420 \rangle$ directions, connecting two LRO positions of the same variant. Careful measurements made of the positions of the diffuse intensity maxima indicate that they coincide with the $\frac{1}{5}\{420\}$ positions in agreement with Thomas and coworkers, [1, 17] (cf. ref. 22). It should be noted that the LRO spots arise from the streaks and that they do not result from equal amplitudes of $\frac{1}{4}\{420\}$ concentration waves (*cf.* Ref. 23). The streaks to the LRO positions are observed when the SRO spots are much more intense than the streaks or the diffracted intensity at the LRO positions. Since the SRO structure exists throughout the alloy and since the superlattice reflections form by a continuous transfer of intensity from the SRO to the LRO positions, the transformation at 700°C is seen to occur continuously or homogeneously. Specifically, since the initial SRO structure is not the same as the final equilibrium one, the transformation mechanism is termed spinodal ordering, as defined by de Fontaine [9]. His model of the continuous formation of the LRO structure from the SRO structure is particularly attractive for this system. He considers the SRO state to be composed of ordering waves with a **k**-vector of $\frac{1}{4}\langle 420 \rangle$, which change continuously to the $\frac{1}{5}\langle 420 \rangle$ of the LRO state.

In the mechanism of spinodal ordering short wavelength concentration waves become unstable below a certain instability temperature. Such a process occurs by having several intermediate ordering waves present thereby giving rise to several corresponding wave numbers in **k**-space. Since the regions of changing order are small in real space, and since several wave numbers exist, the intensity in reciprocal space would extend along the $\langle 420 \rangle$ directions. A similar model has been previously discussed by Okamoto [23].

This mechanism for an off-stoichiometric alloy would necessarily include phase separation. The manner whereby distinct ordered precipitates form after or concomitant with the homogeneous ordering transformation is not certain. It could occur by (1) nucleation at preferred sites in the matrix where the LRO parameter is higher than that in the average alloy; (2) by spinodal clustering; or (3) by some other continuous process. The exact manner probably cannot be ascertained by CTEM techniques. Lattice imaging may be the best approach to the solution of this problem.

IV. CONCLUSIONS

1. The nature of the SRO intensity maxima support a statistical thermodynamic model for their existence rather than a microdomain model in that the SRO intensity contours remained spherical throughout the transformation process. This result is consistent with the interpretation that the SRO spots result from a minimum in $V(k)$ at the special points $\{1\frac{1}{2}0\}$ in reciprocal space.

2. At 750°C, a heterogeneous transformation occurs by the mechanism of homogeneous nucleation. The following sequence of transformation events takes place at 750°C. (a) Development of the SRO intensity maxima from the as-quenched configuration. (b) The sudden appearance of the LRO intensity maxima at the $\frac{1}{5}\{420\}$ positions in reciprocal space, accompanied by the observation of distinct Ni_4Mo precipitates in direct space. (c) The disappearance of the SRO intensity maxima, and the growth of the Ni_4Mo precipitates.

3. At 700°C, a homogeneous transformation occurs by the mechanism of spinodal ordering. The following sequence of transformation events takes place at 700°C. (a) Development of the SRO intensity maxima from the as-quenched configuration. (b) Streaks between LRO positions of the same variant on the [112] diffraction pattern, but not on the [001] diffraction pattern. (c) Diffuse intensity between the SRO and the LRO positions on the [001] and on the [112] diffraction patterns, accompanied by the formation of the {110} tweed microstructure. (d) Distinct SRO and LRO intensity maxima in reciprocal space and a well-developed tweed microstructure in direct space. (e) Disappearance of the SRO intensity maxima and growth of the Ni_4Mo precipitates into an aligned, periodic microstructure.

4. Aging at 700°C results in coherent Ni_4Mo precipitates elongated in the $[001]_\alpha$ direction, faceted on the $(100)_\alpha$ and $(010)_\alpha$ planes and periodically aligned in the $[100]_\alpha$ and $[010]_\alpha$ directions.

Acknowledgements—We would like to thank Drs. J. W. Cahn, A. G. Khachaturyan, F. W. Ling, R. Sinclair, W. A. Soffa and Lee Tanner for some very stimulating and helpful discussions. L. A. Nesbit was supported for part of the investigation by a Rockwell Fellowship, and D. E. Laughlin was supported by two grants from The National Science Foundation, Division of Materials Research (75-10818, 76-22353).

REFERENCES

1. P. R. Okamoto and G. Thomas, *Acta Met.* **19**, 825 (1971).
2. J. W. Gibbs, *Scientific Papers*, Vol. 1. Dover, New York (1961).
3. J. W. Christian, *The Theory of Transformations in Metals and Alloys.* Pergamon Press, Oxford (1975).
4. R. Sinclair, J. A. Leake, and B. Ralph, *Phys. Status Solidi (A)* **26**, 285 (1974).
5. D. E. Laughlin and J. W. Cahn, *Metall. Trans.* **5**, 492 (1974).
6. D. E. Laughlin and J. E. Cahn, *Acta Met.* **23**, 329 (1975).
7. A. Datta and W. A. Soffa, *Acta Met.* **24**, 987 (1976).
8. L. E. Tanner and D. E. Laughlin, *Scripta Met.* **9**, 373 (1975).
9. D. de Fontaine, *Acta Met.* **23**, 553 (1975).

10. D. de Fontaine in *Ultrafine-Grain Metals* (edited by J. J. Burke and V. Weiss). Syracuse University Press, Syracuse, New York (1970).
11. P. V. Guthrie and E. E. Stansbury, *ORNL* 3078 *USAEC* (1961).
12. E. Ruedl, P. Delavignette, and S. Amelinckx, *Phys. Status Solidi* **28,** 305 (1968).
13. E. Spruiell, L. M. Ruch, and C. R. Brooks, *Metall. Trans.* **A6,** 1301 (1975).
14. L. E. Tanner, *Acta Met.* **20,** 1197 (1972).
15. S. K. Das, P. R. Okamoto, P. M. J. Fisher, and G. Thomas, *Acta Met.* **21,** 913 (1973).
16. S. K. Das and G. Thomas, in *Order–Disorder Transformations in Alloys* (edited by H. Warlimont). Springer, New York (1974).
17. G. Thomas and R. Sinclair, *Acta Met.* **25,** 231 (1977).
18. P. C. Clapp and S. C. Moss, *Phys. Rev.* **171,** 754 (1968).
19. S. C. Moss and P. C. Clapp, *Phys. Rev.* **171,** 764 (1968).
20. B. Chakravarti, E. A. Starke, C. J. Sparks, and R. O. Williams, *J. Phys. Chem. Solids* **35,** 1317 (1974).
21. R. DeRidder, G. Van Tendeloo, and S. Amelinckx, *Acta crystallogr.* **A32,** 216 (1976).
22. J.-P. A. A. Chevalier and W. M. Stobbs, *Acta Met.* **24,** 535 (1976).
23. P. R. Okamoto, Ph.D. Thesis, University of California, Berkeley. UCRL-19175 (1970).